J Mol Model (2015) 21: 314
DOI 10.1007/s00894-015-2855-2

ORIGINAL PAPER

Ensembling and filtering: an effective and rapid in silico multitarget drug-design strategy to identify RIPK1 and RIPK3 inhibitors

S. M. Fayaz[1,2] · **G. K. Rajanikant**[1]

Received: 28 August 2015 / Accepted: 2 November 2015 / Published online: 20 November 2015

Abstract Necroptosis, a programmed necrosis pathway, is witnessed in diverse human diseases and is primarily regulated by receptor-interacting serine/threonine protein kinase 1 (RIPK1) and RIPK3. Ablation or inhibition of these individual proteins, or both, has been shown to be protective in various in vitro and in vivo disease models involving necroptosis. In this study, we propose an effective and rapid virtual screening strategy to identify multitarget inhibitors of both RIPK1 and RIPK3. It involves ensemble pharmacophore-based screening (EPS) of a compound database, post-EPS filtration (PEPSF) of the ligand hits, and multiple dockings. Structurally diverse inhibitors were identified through ensemble pharmacophore features, and the speed of this process was enhanced by filtering out the compounds containing cross-features. The stability of these inhibitors with both of the proteins was verified by means of molecular dynamics (MD) simulation.

Keywords Ensemble pharmacophore · Ensemble docking · Dual ensemble screening (DES) · Ensemble pharmacophore-based screening (EPS) · Post-EPS filtration (PEPSF) · Dual inhibitors

✉ G. K. Rajanikant
rajanikant@nitc.ac.in

[1] School of Biotechnology, National Institute of Technology Calicut, Calicut 673601, India

[2] Department of Biotechnology, Manipal Institute of Technology, Manipal University, Manipal 576104, Karnataka, India

Introduction

Necroptosis is a programmed necrotic cell death mechanism observed in various human pathologies, such as neonatal brain hypoxia [1], acute pancreatitis [2, 3], cerebral ischemia [4–6], Alzheimer's disease (AD), and Parkinson's disease (PD) [7]. It is also involved in myocardial infarction, retinal injuries, lethal systemic inflammatory response syndrome, skin inflammation, acute pancreatitis, and viral infection [8, 9]. Receptor-interacting serine/threonine protein kinase 1 (RIPK1) and RIPK3 are the two crucial regulatory proteins involved in this pathway [10–13]. In vitro and in vivo studies have established RIPK1 as a specific protein target of the necroptotic pathway [14–18]. Inhibition of RIPK1 leads to reduced necroptotic cell death and increased cell survival rate [14, 19–21].

Genetic studies have revealed that the targeted deletion of RIPK3 would rescue caspase-8 dependent necroptosis and embryonic lethality in mice [13, 22, 23]. Moreover, RIPK3 was suggested as a necroptotic target in RIP1-deficient cells [2, 24]. RIP1-independent and RIP3-dependent necroptosis can occur in RIP1-deficient mouse embryonic fibroblast cells [2] and also in RIP1/caspase-8 double-knockdown L929 cells [24]. Therefore, there is a need to identify dual inhibitors that may target both RIPK1 and RIPK3 proteins. Pharmacological agents that target both the RIPK1 and RIPK3 proteins might offer more effective cellular protection in diseases involving necroptosis. Information regarding the active-site features of these proteins might assist in discovering novel structurally diverse inhibitors. To the best of our knowledge, computational methods have not been used to explore the conformational flexibility of the RIPK3 binding site or to identify RIPK3 inhibitors.

Structure-based pharmacophore modeling is an important event in most in silico drug-design strategies. The use of multiple protein structures for pharmacophore extraction is

considered an improvement over the standard technique of using a single structure. It was proposed that a multicomplex-based pharmacophore model derived from many holoprotein (protein–ligand complex) structures would determine all of the key protein–ligand interactions [25]. In addition, an ensemble pharmacophore derived from multiple apoprotein (protein only) and holoprotein structures was proposed that could extract all of the features available at the binding site of the protein [26]. The screening of multitarget ligands using pharmacophores derived from multiple structures of each protein is the preferred choice, particularly when the conformations of these structures vary considerably and the ligands bind to them with different pharmacophoric features [27]. This could result in the effective screening of compounds with different scaffolds.

In general, the pharmacophores derived from multiple structures of a protein are combined to develop a merged pharmacophore or an ensemble pharmacophore in order to decrease the number of pharmacophore-based screenings and to reduce the computational time [26, 27]. These pharmacophores contain all of the features present at the binding sites of individual structures. Compound screening using these pharmacophores could highlight ligands that contain the features of individual structures. However, ligands that contain a combination of features present in different structures might also be obtained, which increases the number of false positives enormously (Fig. 1). The presence of these unwanted compounds with "cross-features" of multiple structures might in turn lead to increased docking time and a greater computational load. Therefore, there is a need to filter out these compounds before preparing the final ligand dataset for docking.

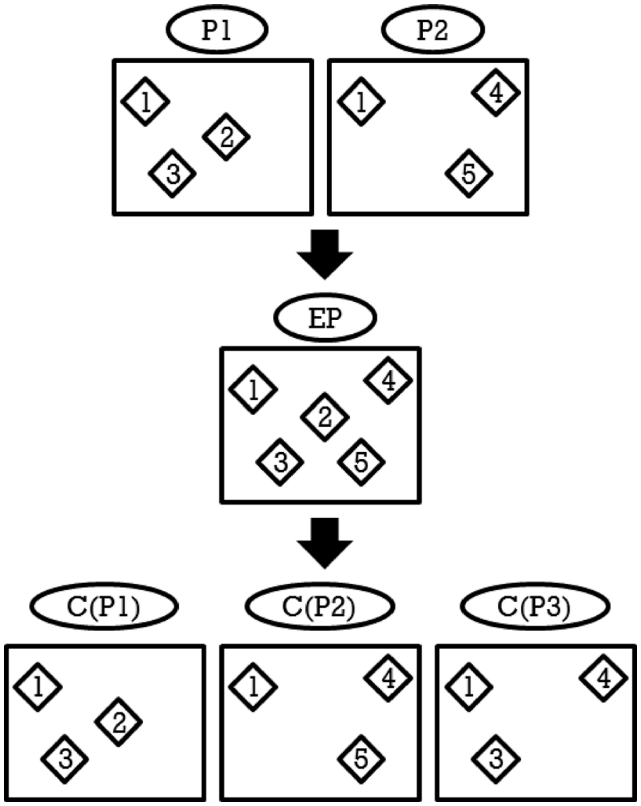

Fig. 1 Limitation of a merged or ensemble pharmacophore. C(P1) and C(P2) are groups of compound hits that contain the features of the pharmacophores P1 and P2, respectively. C(P3) is a group of false-positive compounds that contain features of both pharmacophores ("cross-features")

For instance, assume that a hypothetical protein contains two structures with different conformations; P1 and P2 are the pharmacophores derived from them, respectively (Fig. 1). P1 contains features 1, 2, and 3. P2 contains features 1, 4, and 5. A merged pharmacophore or an ensemble pharmacophore (EP) derived by combining these two pharmacophores contains features 1, 2, 3, 4, and 5 (Fig. 1). Theoretically, screening a compound dataset using this EP should result in two groups of compound hits, C(P1) and C(P2), with the features of any of the two pharmacophores P1 and P2. However, in practice, in addition to these two groups of compound hits, a group of unwanted compounds denoted C(P3) can be obtained that contain cross-features of P1 and P2, e.g., 1, 3, and 4 (Fig. 1). Employing these compounds in the subsequent docking step could increase both the computational time and load.

In the study reported in the present paper, we derived two ensemble pharmacophores, one from the RIPK1 protein structures in the PDB and the other from the modeled protein structures of RIPK3 (Fig. 2). At first, ensemble pharmacophore-based screening (EPS) of ZINC database compounds was carried out using the RIPK1 ensemble pharmacophore. The compound hits thus obtained could contain cross-features. Therefore, in this work we propose a novel method that we call post ensemble pharmacophore-based screening filtration (PEPSF), and we used this method to separate the compound hits into groups that each contain features of an individual pharmacophore (Fig. 2). The compounds excluded by PEPSF contained cross-features and were not considered for further analysis. Next, these groups of compounds were subjected to EPS using RIPK3 EP. Then, PEPSF was carried out on the compound hits, leading to different groups of compounds containing pharmacophore features of both the RIPK1 and RIPK3 proteins. These groups of compounds were subjected to multiple dockings with their corresponding RIPK1 and RIPK3 protein structures (Fig. 2). Finally, MD simulation was carried out to study the behavior of the top-ranking RIPK1 and RIPK3 dual inhibitors. This strategy allows effective multitarget inhibitors to be rapidly identified, since it removes the false-positive compounds and greatly reduces the number of compounds that are virtually screened, thereby minimizing the computational time and load.

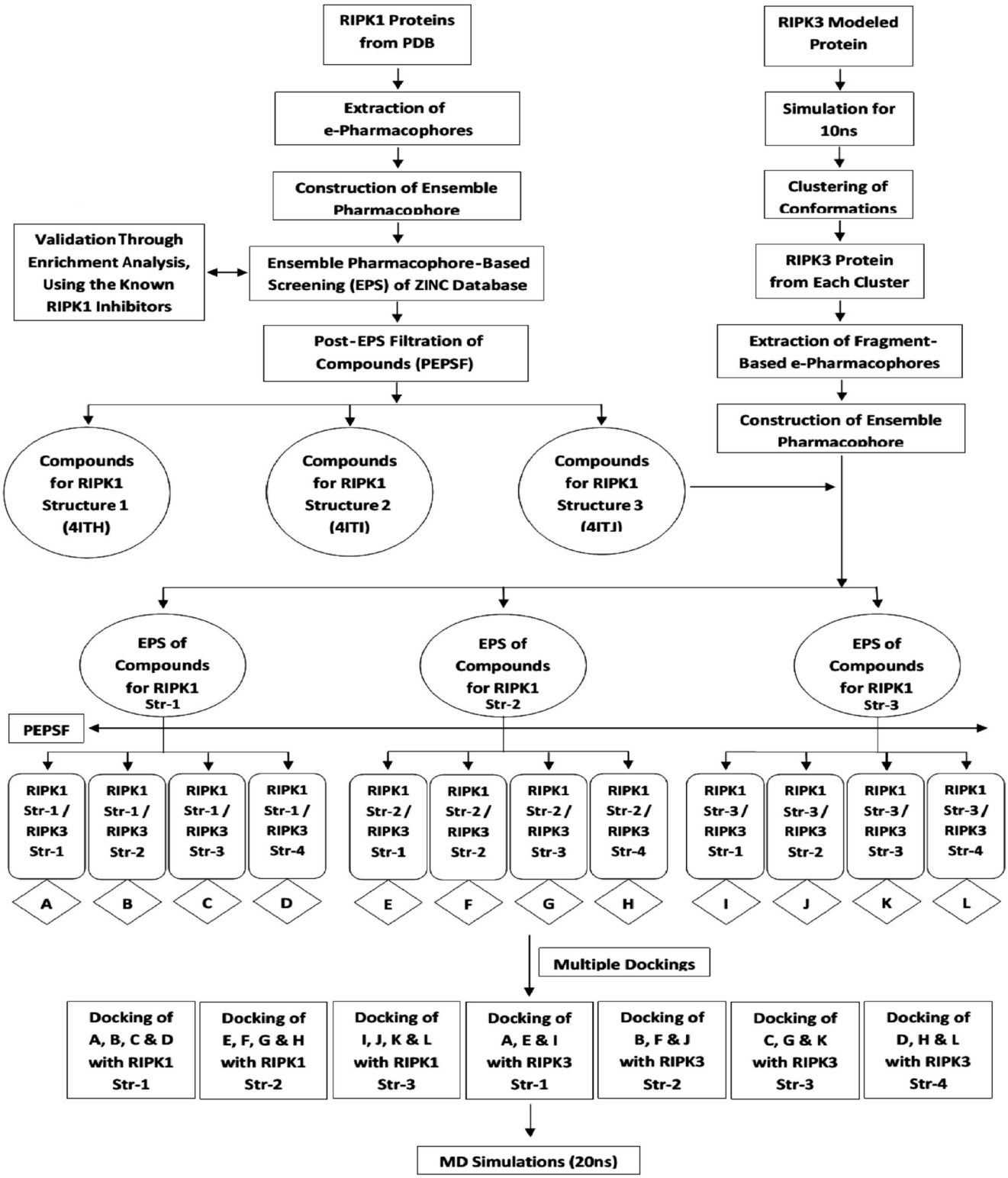

Fig. 2 Workflow used in this study to identify RIPK1 and RIPK3 dual inhibitors. An ensemble pharmacophore was derived from RIPK1 structures and validated, and this was employed to screen the database compounds. The compound hits were subjected to PEPSF, leading to three groups of ligands, with each group corresponding to the pharmacophore features of each RIPK1 structure. These ligands were screened using the RIPK3 ensemble pharmacophore. The ligand hits thus obtained were subjected to PEPSF, yielding 12 groups. These ligands then underwent multiple dockings, and MD simulations were carried out on the top-ranked protein–ligand complexes

Methods

RIPK1 protein structures

The protein–ligand complexes of RIPK1 were retrieved from the PDB (PDB IDs: 4ITH, 4ITI, and 4ITJ) and were prepared using the protein preparation wizard of Schrodinger (Schrodinger, LLC, New York, NY, USA). Missing hydrogens were added, proper bond orders were assigned, and water molecules further than 5 Å from the heterogeneous groups were deleted. The H-bonds were optimized and the protein structures were minimized to the default root mean square deviation (RMSD) value of 0.30 Å. The minimized protein structures were further considered for pharmacophore analysis and docking.

RIPK3 protein structure modeling

The protein sequence of the kinase domain of human RIPK3 was retrieved from the UniProt database (ID: Q9Y572). Homology modeling of the 3D structure of RIPK3 was carried out using the Prime v2.2 module of the Schrodinger suite (Schrodinger, LLC). Side chains and hydrogen atoms were added and the stability of the homology model was validated through PROCHECK and the Ramachandran plot hosted by the Structural Analysis and Verification Server (SAVES) (http://nihserver.mbi.ucla.edu/SAVS/).

MD simulation and clustering

To obtain diverse conformations, the modeled RIPK3 protein was subjected to MD simulation using the Gromacs v.4.5.5 software package with the Gromos 53a6 force field, as described previously [26].

Prior to executing the MD simulation, 20,000 steps of steepest descent minimization in vacuum were carried out on the system, followed by explicit solvation in a cubic box containing simple point charge (SPC/E) water molecules. During the preparation procedure for the MD simulation, the ionizable residues of the protein were protonated without artifacts and the system was neutralized by the addition of Na^+ and Cl^- counterions and a salt concentration of 0.1 M NaCl. All of the hydrogen-related bond lengths were fixed with the Linear Constraint Solver (LINCS) algorithm, and the long-range electrostatic interactions were treated with the Particle Mesh Ewald (PME) method [28]. Further, all of the bond lengths involving H-atoms were constrained using the SHAKE algorithm, and the solvated system was subjected to 20,000 steps of steepest descent energy minimization. Then the system was equilibrated for 100 ps with an NVT and NPT ensemble equilibration protocol for about 50,000 steps. Finally, extensive MD simulation was performed for 10 ns with a 2.0-fs time step under constant temperature and pressure (310 K and 1 bar, respectively).

Clusters were generated by comparing the root mean square deviation (RMSD) cutoff values obtained for different snapshots during the MD simulation trajectory. The energy of each conformation was compared with the lowest energy within the trajectory to estimate the relative possibility of the conformation. Finally, representative structures that were closest to the average conformation were selected from each of the clusters. These protein structures were prepared as described in the previous section, and were considered for RIPK3 pharmacophore analysis and docking.

Receptor grid generation and docking

Glide energy grids were generated for all of the prepared protein structures. In the case of RIPK1, the co-crystallized ligand was differentiated from the active site of the receptor. The grid was defined by a rectangular box surrounding the co-crystallized ligand. For RIPK3 structures, the grid was generated such that it covered the active site of the protein. These grids were employed in all of the docking studies.

Docking was performed with the Glide module using the OPLS 2005 force field [29]. Default settings were selected for all of the docking calculations, and the Glide XP descriptor information was used to deduce energy terms such as H-bond interactions, electrostatic interactions, hydrophobic enclosure, and π–π stacking interactions (Glide v.5.7, Schrodinger, LLC). Finally, post-docking minimization was carried out to optimize the ligand geometries.

E-pharmacophore extraction

Structure-based pharmacophores were extracted from RIPK1 and RIPK3 protein structures using the energy-optimized pharmacophore (e-pharmacophore) script of Schrodinger [30]. Fragment-based e-pharmacophores were extracted from RIPK1 and RIPK3 protein structures.

For fragment-based e-pharmacophore extraction, the Glide fragment library was docked to each of the proteins using Glide XP. The resultant pose viewer files were used in both cases to generate pharmacophores via the e-Pharmacophore script in the Schrodinger software. A standard set of six pharmacophore features, i.e., H-bond acceptors (A), H-bond donors (D), hydrophobic groups (H), negatively ionizable regions (N), positively ionizable regions (P), and aromatic rings (R), were generated with the Phase module. The generated pharmacophore sites were ranked based on their energies, and the most favorable sites were selected for the pharmacophore hypothesis.

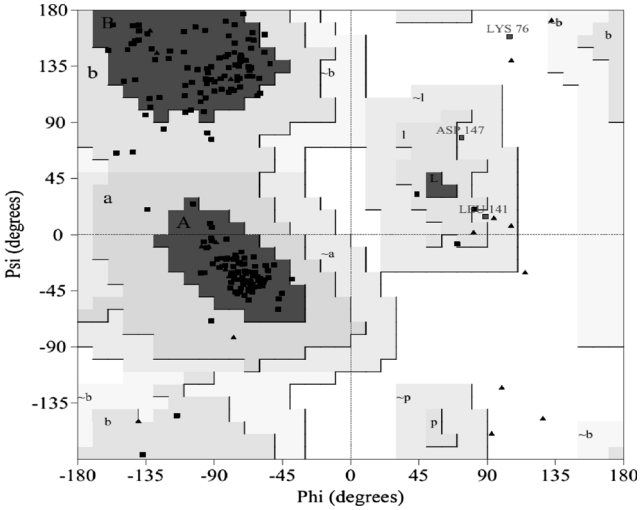

Fig. 3 Ramachandran plot of the modeled RIPK3 protein structure

Ensemble pharmacophore construction

The e-pharmacophores extracted from the RIPK1 proteins were superposed and they were combined to generate an ensemble pharmacophore, as described previously [26]. Similarly, fragment-based e-pharmacophores extracted from RIPK3 proteins were combined to build an ensemble pharmacophore. The ensemble pharmacophore contained all of the features that the individual e-pharmacophores had in common, as well as the features that varied among the e-pharmacophores. If common features relating to the same amino acid at the binding site were present, they were considered a single feature, so only one of them was represented in the ensemble pharmacophore.

RIPK1 ensemble pharmacophore-based screening

Ensemble pharmacophore-based screening (EPS) of RIPK1 was carried out by employing its ensemble pharmacophore to screen the lead-like compounds (~2 million unique structure records) in the ZINC database [31] using the Phase module. The database molecules were filtered explicitly with a distance-matching tolerance of 2.0 Å, and matching of a minimum of four sites was required. The database hits were ranked based on their fitness scores, which measured how well the aligned ligand conformers matched the hypothesis.

The RIPK1 ensemble pharmacophore was validated using the enrichment factor (EF). The enrichment at a given percentage of the database screened is the most popular and the simplest metric method used to evaluate the effectiveness of a virtual screening method [32, 33]. The EF is defined as

$$\mathrm{EF}^{x\%} = \frac{n(\text{active at } x\%)/n(x\%)}{n(\text{all active})/n(\text{all})},$$

where n(active at x%) is the number of active ligands obtained in the top x% of the database screened, $n(x\%)$ is the number of compounds screened in the top x% of the database, n(all active) is the number of active ligands in the entire database, and n(all) is the number of compounds in the entire database [34].

All of the known RIPK1 inhibitors were randomly seeded into the ZINC database and EPS was carried out on these compounds, as described previously [26].

RIPK1 post-EPS filtration

The compound hits obtained through EPS contained the features of individual pharmacophores. However, false-positive compounds that contained cross-features were also present. In order to filter out these compounds, PEPSF was carried out, which separated the compounds into groups with features from individual pharmacophores.

The output of RIPK1 EPS obtained using Phase, when viewed in the form of a table, contained a column named "matched ligand sites." This gave information on the pharmacophore features present in each compound hit that matched with the RIPK1 ensemble pharmacophore features. This table was exported in the form of an Excel worksheet, and the compound hits were sorted based on their matching sites. These sites were compared with each of the RIPK1 fragment-based e-pharmacophores, and the compounds with sites that matched with any of these pharmacophores were considered. Compounds with sites that matched with more than one pharmacophore were considered false positives since they contained cross-features, and were removed from the study. Thus, each of the three RIPK1 fragment-based e-pharmacophores had a corresponding group of compounds containing features

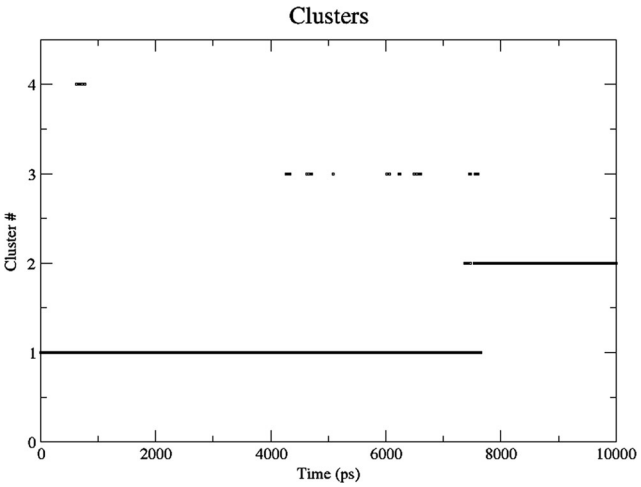

Fig. 4 Clusters of the RIPK3 protein conformations produced during MD simulation

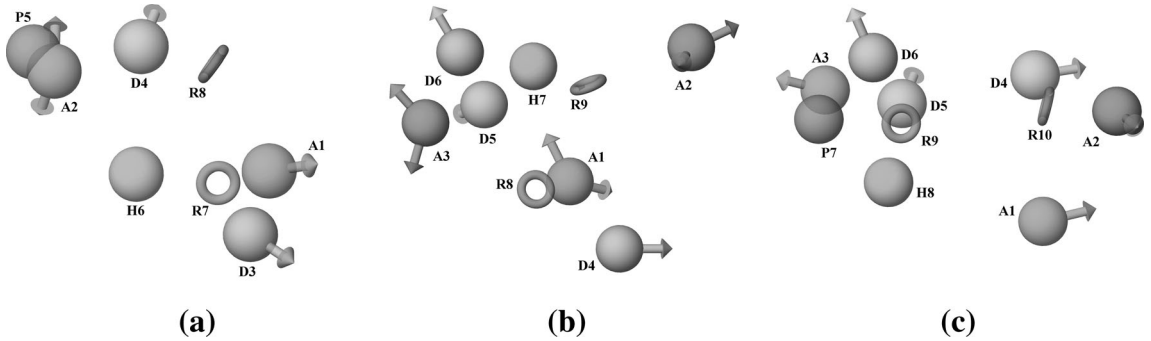

Fig. 5a–c Fragment-based e-pharmacophores derived from the three RIPK1 protein structures: **a** from 4ITH; **b** from 4ITI; **c** from 4ITJ. The letters *A*, *D*, *P*, *H*, and *R* represent acceptor, donor, positive, hydrophobic, and aromatic features, respectively

that were complementary to that e-pharmacophore (i.e., there were three groups in total).

RIPK3 ensemble pharmacophore-based screening

The ensemble pharmacophore of RIPK3 was used to screen the three groups of compounds obtained through RIPK1 PEPSF. This resulted in compound hits that contained the features of both the RIPK1 and RIPK3 proteins. The RIPK3 ensemble pharmacophore could not be evaluated using EF since there were no reported RIPK3 inhibitors when this study was carried out.

RIPK3 post-EPS filtration

In order to remove the compounds that contained cross-features and did not match with any of the four pharmacophores derived from the RIPK3 structures, the compound hits that were obtained through RIPK3 EPS were subjected to PEPSF as described in the previous section.

Docking-based virtual screening

Using RIPK3 PEPSF, the database hits obtained from RIPK3 EPS were separated into different groups that contained

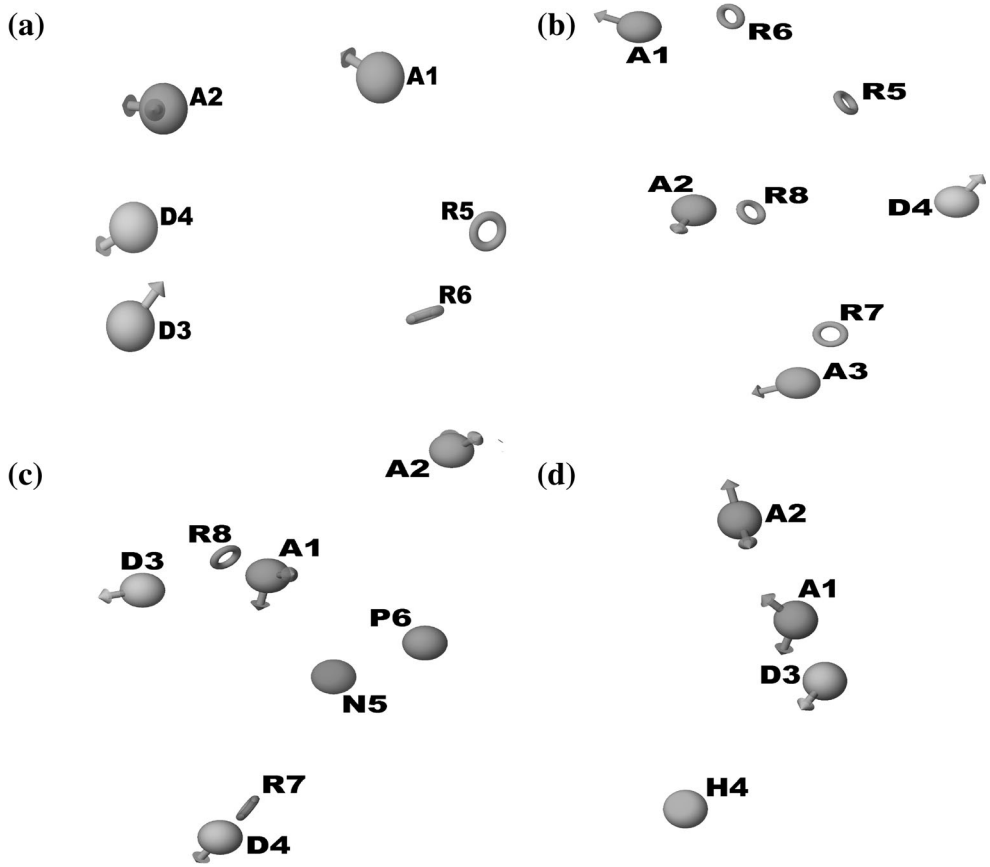

Fig. 6a–d Fragment-based e-pharmacophores derived from the four RIPK3 protein structures: **a** from structure 1; **b** from structure 2; **c** from structure 3; **d** from structure 4. The letters *A*, *D*, *N*, *P*, *H*, and *R* represent acceptor, donor, negative, positive, hydrophobic, and aromatic features, respectively

Table 1 Ensemble pharmacophore features of RIPK1 and their respective three-dimensional coordinates

Serial no.	Feature type	*X*	*Y*	*Z*
1	A	7.824740	15.983200	33.824800
2	A	7.265640	13.183500	28.839200
3	A	3.672600	8.050270	31.424700
4	D	5.046720	13.715600	26.844800
5	D	8.163100	13.501600	34.772400
6	D	9.126590	13.592500	32.194600
7	D	6.011190	13.292500	34.013400
8	D	9.498540	9.196160	30.563600
9	D	3.986080	10.581000	31.127900
10	R	6.656320	14.479300	29.785700
11	R	5.491500	11.227000	32.018400

pharmacophore features of any of the three RIPK1 proteins and also any of the four RIPK3 proteins. Multiple dockings were carried out to study the binding of the compounds in each group with their respective RIPK1 and RIPK3 protein structures (Fig. 2).

Prior to docking, the compounds obtained through RIPK3 PEPSF were subjected to ligand preparation by the LigPrep module of the Schrodinger suite (LigPrep v.2.3, Schrodinger, LLC). The ligands were processed to assign suitable protonation states at a physiological pH of 7.2±0.2, and conformer generation was carried out with ConfGen torsional sampling using the OPLS 2005 force field. Docking was performed using Glide in the Virtual Screening Wizard of the Schrodinger suite. All of the docking calculations were

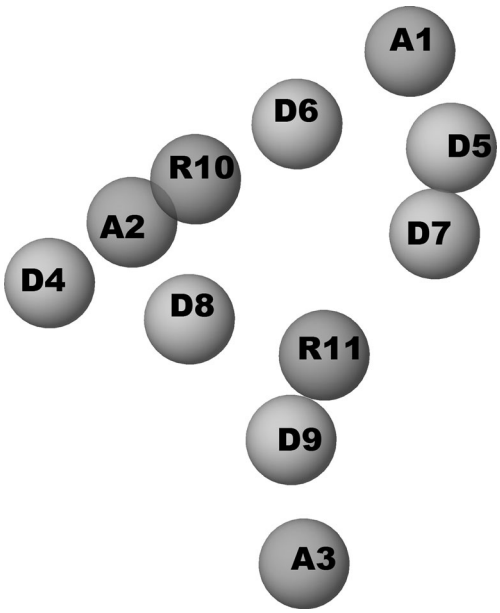

Fig. 7 RIPK1 ensemble pharmacophore derived by combining the three RIPK1 e-pharmacophores. The letters *A*, *D*, and *R* represent acceptor, donor, and aromatic features, respectively

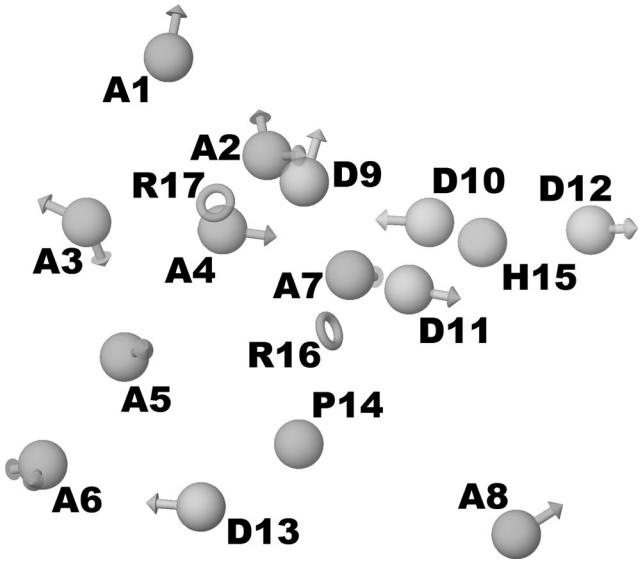

Fig. 8 RIPK3 ensemble pharmacophore derived by combining the four RIPK3 e-pharmacophores. The letters *A*, *D*, *P*, *H*, and *R* represent acceptor, donor, positive, hydrophobic, and aromatic features, respectively

performed as mentioned in an earlier section. The docking results (comprising the compounds listed in the order in which they were docked) as well as the Glide scores were obtained.

MD simulation of lead compounds

Based on the docking results and Glide scores of the compounds that were found to bind to both the RIPK1 and RIPK3 proteins, the top two ranked protein–ligand complexes

Table 2 Ensemble pharmacophore features of RIPK3 and their respective three-dimensional coordinates

Serial no.	Feature type	*X*	*Y*	*Z*
1	A	−17.854900	4.699670	5.512760
2	A	−21.100900	6.663130	12.512200
3	A	−17.649300	9.850000	13.968400
4	A	−24.405700	5.028640	9.613520
5	A	−31.407800	3.542050	2.466110
6	A	−19.846900	3.429170	10.943900
7	A	−15.968300	3.827950	1.667200
8	A	−15.442100	3.027830	10.466900
9	D	−26.151400	2.062590	13.043500
10	D	−26.457000	5.638620	9.271740
11	D	−21.702000	7.217410	−0.037882
12	D	−22.765400	9.025160	10.945400
13	D	−31.143900	0.766501	14.320000
14	P	−23.492900	0.544939	5.266880
15	R	−24.317000	6.240190	7.123050
16	R	−19.670000	5.425350	11.041600
17	H	−28.107200	3.128160	12.297100

Table 3 Output from the docking of the top three ranking lead molecules with the RIPK1 and RIPK3 proteins

Ligand	Zinc ID	Protein target	Glide score	Glide energy	Amino acids involved in H-bond interactions
Lead 1	ZINC01659029	RIPK1	−13.0921	−50.621672	Met 67, Val 76, Asp 156
Lead 2	ZINC71828321	RIPK1	−12.827719	−55.550181	Val 76, Asp 156, Ser 161
Lead 3	ZINC72165687	RIPK1	−13.0261	−52.713718	Leu 70, Ile 154, Asp 156, Ser 161
Lead 1	ZINC01659029	RIPK3	−8.2607	−53.881427	Lys 37, Ser 133
Lead 2	ZINC71828321	RIPK3	−7.6814	−51.311097	Lys 131, Asp 147
Lead 3	ZINC72165687	RIPK3	−8.8929	−50.614867	Ser 133, Asp 147

(RIPK1–lead 1, RIPK3–lead 1, RIPK1–lead 2, and RIPK3–lead 2) were selected to carry out 20-ns MD simulations as described in the earlier section. In addition, the RIPK1–necrostatin-1 (Nec-1) and RIPK3–Nec-1 complexes were subjected to MD simulation to study the binding of Nec-1 with both proteins. The topologies and parameters for the ligands were generated using PRODRG [35]. The Gromacs and Visual Molecular Dynamics (VMD) packages were used to analyze the MD simulation results [36].

Results and discussion

RIPK3 protein

The 3D structure of human RIPK3 protein was modeled using the crystal structure of mouse RIPK3 kinase domain (PDB ID: 4 M66) as the template. The kinase domain of RIPK3 contains approximately 211 amino acids and its sequence is 70 % similar to its mouse counterpart. The Ramachandran plot indicated that 99.5 % of the amino acid residues in the modeled structure are present in the allowed region (Fig. 3).

Clustering of the conformations obtained through MD simulation of the RIPK3 protein produced four clusters (Fig. 4). A representative structure from each cluster was selected, so four RIPK3 protein structures were used in this study.

E-pharmacophores

Fragment-based e-pharmacophores were derived from the three RIPK1 protein structures, as described previously [26]. The fragment-based e-pharmacophore derived from 4ITH consisted of eight features (2A, 2D, 1P, 1H, and 2R) (Fig. 5a); the amino acids Met 67, Leu 70, Val 76, Leu 78, and Asp 156 were H-bond acceptors and donors. The e-pharmacophore derived from 4ITI consisted of nine features (3A, 3D, 1H, and 2R) (Fig. 5b); Leu 70, Val 76, Leu 78, Asp 156, and Ser 161, were the H-bond acceptors and donors. The e-pharmacophore derived from 4ITJ consisted of ten features (3A, 3D, 1P, 1H, and 2R) (Fig. 5c), where Met 67, Leu 70, Val 76, Ile 154, Asp 156, and Ser 161 were the H-bond acceptors and donors. Thus, the fragment-based e-pharmacophores may have identified all of the possible features present at the RIPK1 binding site.

The fragment-based e-pharmacophore derived from RIPK3 structure 1 consisted of six features (2A, 2D, and 2R) (Fig. 6a), where the H-bond acceptors and donors were the amino acids Lys 37, Thr 81, Ala 146, and Glu 47. The e-pharmacophore derived from RIPK3 structure 2 consisted of eight features (3A, 1D, and 4R) (Fig. 6b); Gly 17, Asp 147, Met 84, and Arg 46 were the H-bond acceptors and donors. The e-pharmacophore derived from RIPK3 structure 3 consisted of eight features (2A, 2D, 1 N, 1P, and 2R) (Fig. 6c), where the H-bond acceptors and donors were Gly

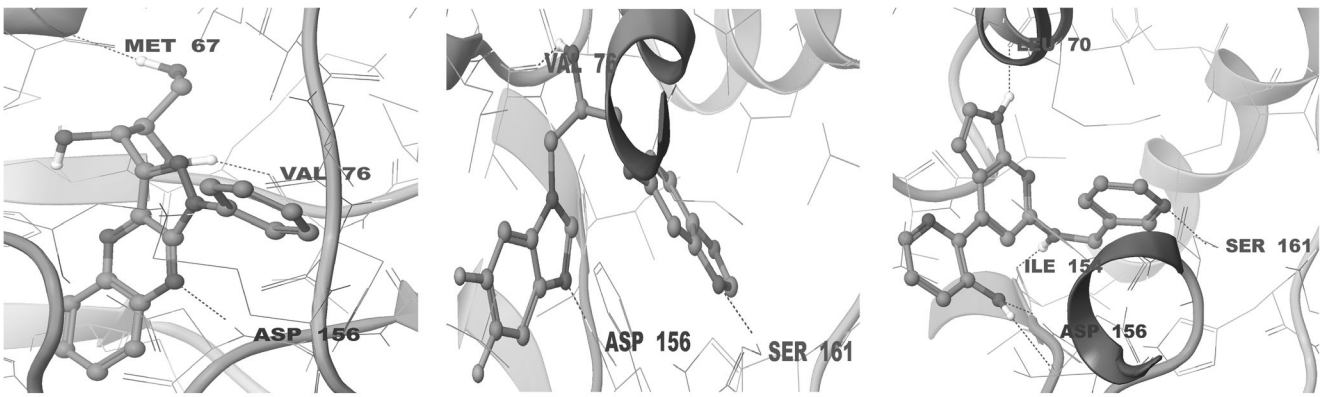

Fig. 9a–c Output from the docking of the top-ranking ligands with RIPK1: **a** ligand ZINC01659029; **b** ligand ZINC71828321; **c** ligand ZINC72165687

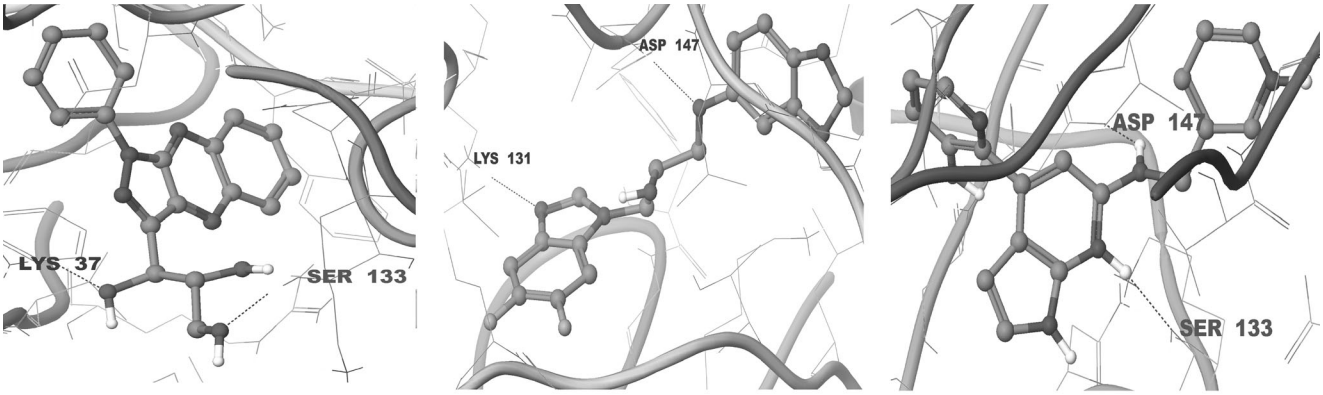

Fig. 10a–c Output from the docking of the top-ranking ligands with RIPK3: **a** ligand ZINC01659029; **b** ligand ZINC71828321; **c** ligand ZINC72165687

17, Lys 131, Thr 81, Ala 50, Lys 37, Asp 129, and Asp 147, while the e-pharmacophore derived from RIPK3 structure 4 consisted of four features (2A, 1D, and 1H) with Ser 133, Lys 131, and Asp 147 as H-bond acceptors and donors (Fig. 6d).

Ensemble pharmacophores

The ensemble pharmacophore of RIPK1 was created by combining all of the fragment-based e-pharmacophore features derived from the three RIPK1 proteins, as described previously [26]. It consisted of eleven features (3A, 6D, and 2R) (Table 1) corresponding to the amino acids Met 67, Leu 70, Val 76, Leu 78, Ile 154, Asp 156, and Ser 161 (Fig. 7). Thus, this ensemble pharmacophore covered all of the important amino acids at the binding site of RIPK1 that may be involved in protein–ligand interactions.

The ensemble pharmacophore of RIPK1 was validated using the early enrichment factors at 1 and 5 % of the database screened. $EF^{1\%}$ and $EF^{5\%}$ were 30 and 8, respectively, indicating that the ensemble pharmacophore contained the features present in the active ligands.

The RIPK3 ensemble pharmacophore was constructed by combining all of the fragment-based e-pharmacophore features extracted from the four RIPK3 protein structures. It

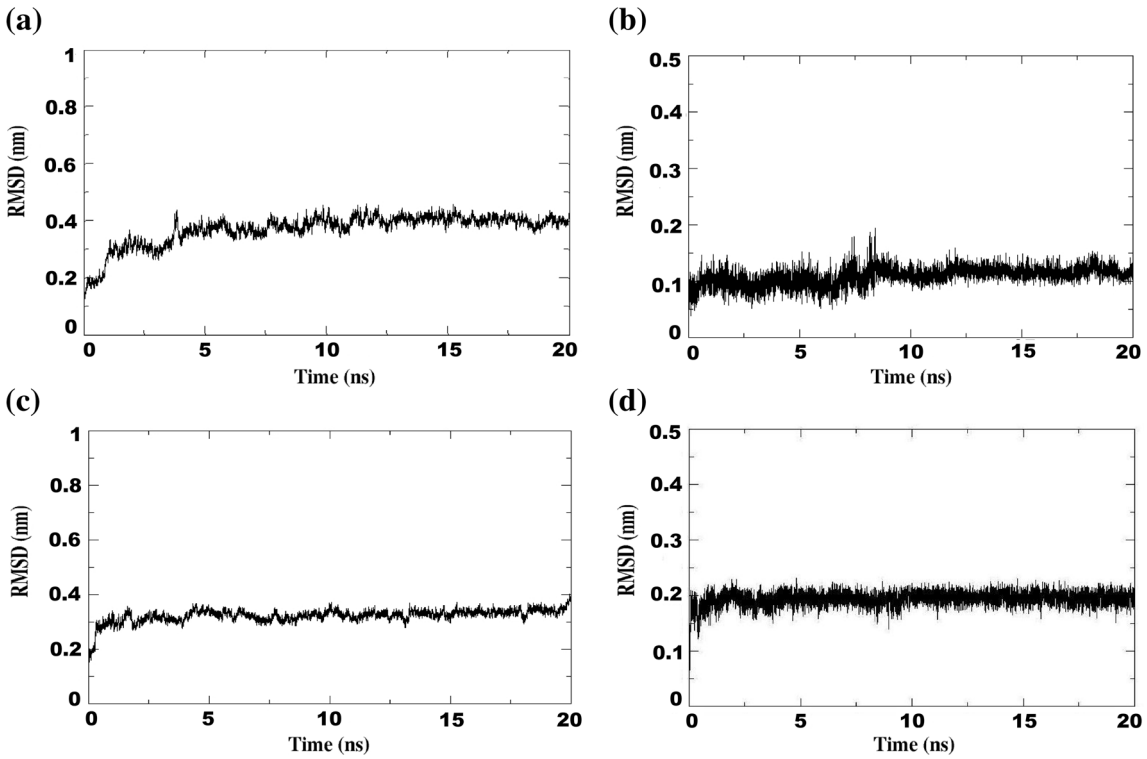

Fig. 11a–d MD simulation results for the binding of lead 1 to the RIPK1 and RIPK3 proteins: **a** RMSD of the RIPK1 protein; **b** RMSD of the lead 1 with RIPK1; **c** RMSD of the RIPK3 protein; **d** RMSD of lead 1 with RIPK3

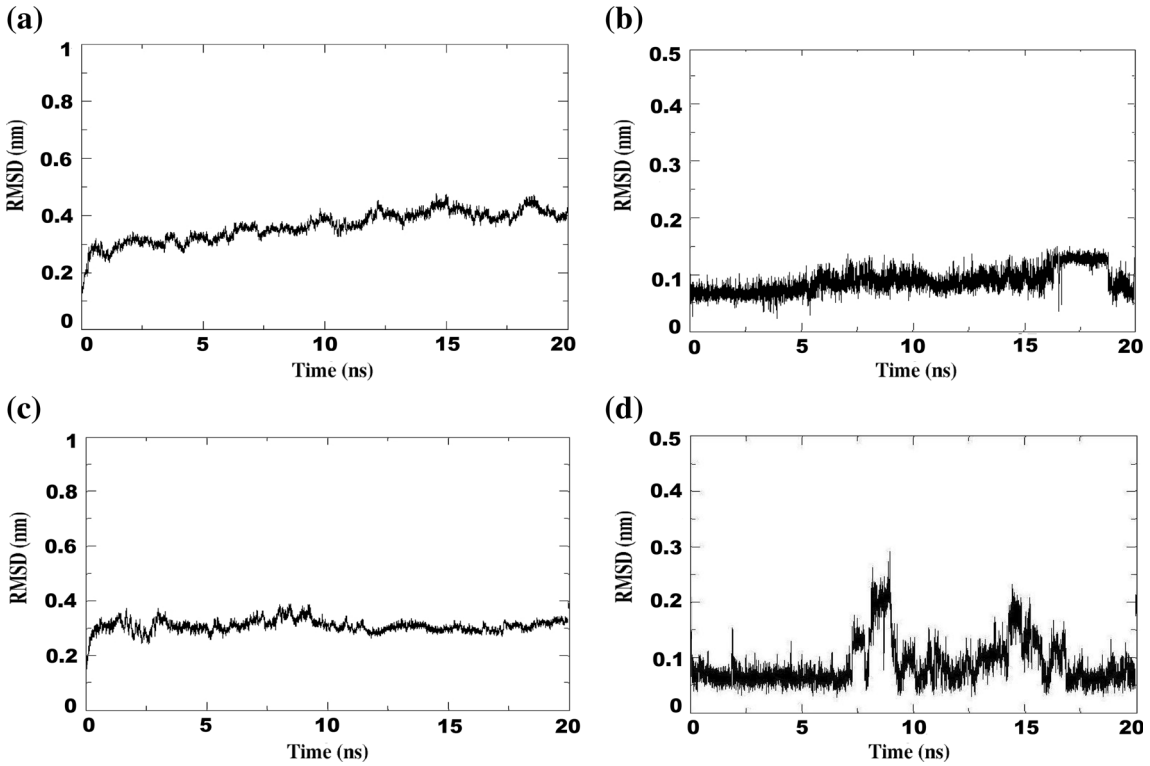

Fig. 12a–d MD simulation results for the binding of lead 2 to the RIPK1 and RIPK3 proteins: **a** RMSD of the RIPK1 protein; **b** RMSD of lead 2 with RIPK1; **c** RMSD of the RIPK3 protein; **d** RMSD of lead 2 with RIPK3

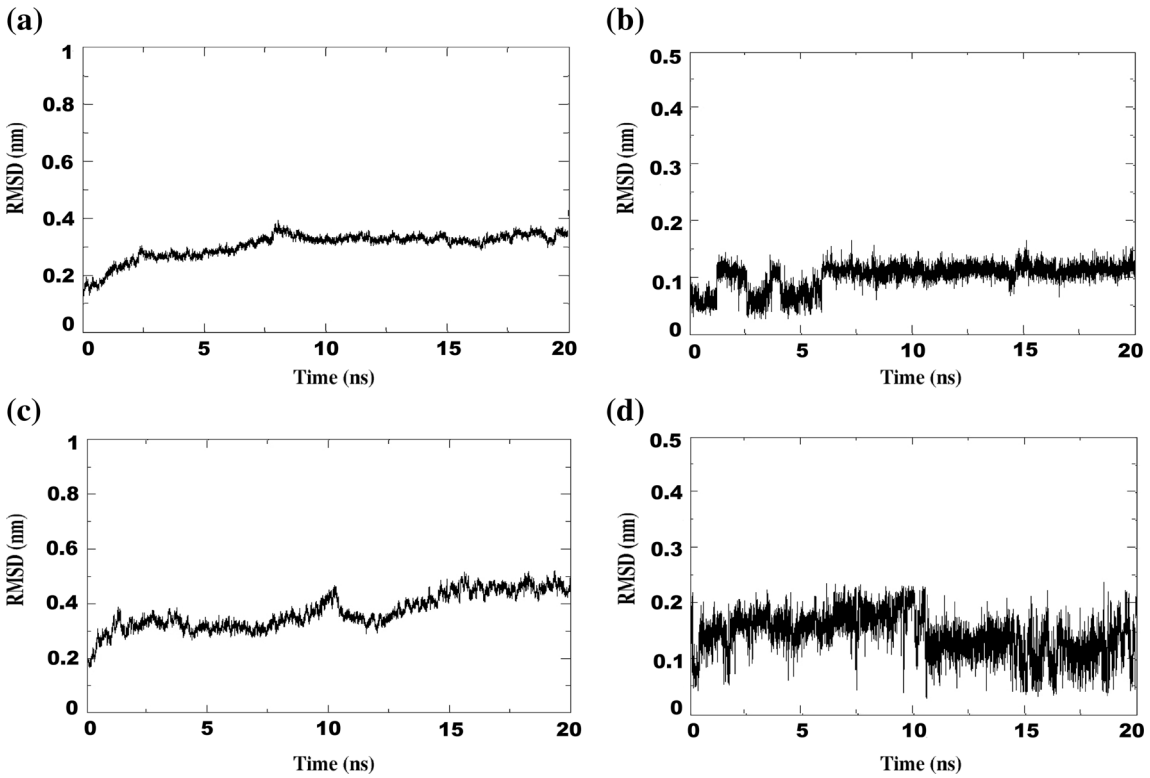

Fig. 13a–d MD simulation results for the binding of Nec-1 to the RIPK1 and RIPK3 proteins: **a** RMSD of the RIPK1 protein; **b** RMSD of Nec-1 with RIPK1; **c** RMSD of the RIPK3 protein; **d** RMSD of Nec-1 with RIPK3

consisted of seventeen features (8A, 5D, 1P, 1H, and 2R) (Fig. 8) (Table 2) corresponding to the amino acids Gly 17, Lys 37, Arg 46, Glu 47, Ala 50, Thr 81, Met 84, Asp 129, Lys 131, Ser 133, Ala 146, and Asp 147. Thus, the pharmacophore features corresponding to all of the important amino acids in the RIPK3 protein structures that might interact with the ligands were retrieved through the ensemble pharmacophore.

RIPK1 EPS and PEPSF

The RIPK1 ensemble pharmacophore was employed to screen the ZINC database of compounds. Approximately 750,000 compound hits were retrieved, which were subjected to PESF. This resulted in 450,000 compounds. PEPSF eliminated nearly 300,000 of those compounds, greatly reducing the computational time required for the docking step.

RIPK3 EPS and PEPSF

The compounds retrieved through RIPK1 PEPSF were subjected to RIPK3 EPS and PEPSF. Approximately 300,000 compounds were retrieved through EPS and 100,000 compounds were obtained after PEPSF. These compounds could contain pharmacophore features of both RIPK1 and RIPK3 and did not harbor any cross-features. Interestingly, Nec-1 exhibited pharmacophore features of the RIPK1 protein only. Finally, applying PEPSF yielded 12 groups of compounds (Fig. 2): group 1 contained pharmacophore features of RIPK1 protein 1 and RIPK3 protein 1, group 2 contained features of RIPK1 protein 1 and RIPK3 protein 2, group 3 contained features of RIPK1 protein 1 and RIPK3 protein 3, group 4 contained features of RIPK1 protein 1 and RIPK3 protein 4, group 5 contained features of RIPK1 protein 2 and RIPK3 protein 1, group 6 contained features of RIPK1 protein 2 and RIPK3 protein 2, group 7 contained features of RIPK1 protein 2 and RIPK3 protein 3, group 8 contained features of RIPK1 protein 2 and RIPK3 protein 4, group 9 contained features of RIPK1 protein 3 and RIPK3 protein 1, group 10 contained features of RIPK1 protein 3 and RIPK3 protein 2, group 11 contained features of RIPK1 protein 3 and RIPK3 protein 3, and group 12 contained features of RIPK1 protein 3 and RIPK3 protein 4.

Multiple dockings

Different groups of compounds were subjected to multiple dockings with their respective RIPK1 and RIPK3 protein structures (Fig. 2). The resultant top-ranked compounds showed good fitness and Glide scores and also exhibited good interactions with the desired amino acids of both the RIPK1 and RIPK3 proteins (Table 3). Lead 1 showed H-bonds with the Met 67, Val 76, and Asp 156 amino acids of RIPK1 (Fig. 9a), and with Lys 37 and Ser 133 of RIPK3 (Fig. 10a). Lead 2 showed H-bonding with Val 76, Asp 156, and Ser 161 of RIPK1 (Fig. 9b), and with Lys 131 and Asp 147 of RIPK3 (Fig. 10b). Similarly, lead 3 exhibited H-bonds with Leu 70, Ile 154, Asp 156, and Ser 161 of RIPK1 (Fig. 9c), and with Ser 133 and Asp 147 of RIPK3 (Fig. 10c). All of the amino acids of RIPK1 and RIPK3 that formed H-bonds with the lead compounds complemented the features present in their respective ensemble pharmacophores.

Validation of leads

The binding and interaction of the top two ranked leads with the RIPK1 and RIPK3 proteins were validated through MD simulation studies. These leads remained in the binding sites of each protein throughout the simulations. The potential energy and the backbone RMSD for each protein and for each ligand complexed with each protein were steady and they stabilized during the course of the simulation (Figs. 11 and 12). However, Nec-1 was only found to bind to RIPK1; this complex remained stable throughout the simulation. It did not bind to RIPK3, so the corresponding complex was not stable during the simulation. This indicates that Nec-1 may not inhibit RIPK3 (Fig. 13), in line with a previous study which reported that Nec-1 only inhibits RIPK1, not RIPK3 [19]. This result represents a validation that the compounds identified using our strategy may inhibit both RIPK1 and RIPK3.

Conclusions

Emerging evidence has confirmed that necroptosis does not necessarily require the interaction of RIPK1 and RIPK3 and the formation of a RIPK1–RIPK3 complex. Both of these proteins can instigate cell death independently, and are thus important targets in neurological disorders. In this study, a novel strategy involving multiple ensemble pharmacophores, PEPSF, and multiple dockings was developed to identify inhibitors of both RIPK1 and RIPK3. Recent studies have reported that employing multiple structures, with different conformations, of a single protein may permit the identification of structurally diverse potential inhibitors. Merged pharmacophores and ensemble pharmacophores are derived from these structures in order to minimize the screening time, since the compound database can be screened in a single step (rather than needing to screen the compounds multiple times, which is necessary when using multiple pharmacophores). However, the compound hits may include numerous false positives with cross-features; docking these false positives may result in a great deal of wasted computational time. Consequently, the computational time that was saved by using merged pharmacophores and ensemble pharmacophores could be lost at the docking phase. PEPSF is able to circumvent this problem by filtering

out all of the false positives and grouping the compounds according to individual pharmacophores.

The top-ranked compounds identified in the present study had pharmacophore features that were complementary to the binding sites of both RIPK1 and RIPK3. These compounds exhibited stable interactions and formed stable complexes with both proteins throughout the course of each MD simulation. Further, Nec-1 could only bind to RIPK1; it did not form a stable complex with RIPK3. Therefore, the present strategy might facilitate the rapid in silico identification of effective multitarget inhibitors, and the compounds identified in this study may prove to be potential RIPK1 and RIPK3 dual inhibitors.

Compliance with ethical standards

Conflict of interest The authors declare that they have no conflict of interest.

Funding This study was funded by the Department of Biotechnology, Government of India via the Bioinformatics Infrastructure Facility for Biology Teaching through Bioinformatics (BIF-BTBI) (grant number: BT/BI/25/001/2006, dated 25/03/2011).

References

1. Thornton C, Rousset CI, Kichev A, Miyakuni Y, Vontell R, Baburamani AA, Fleiss B, Gressens P, Hagberg H (2012) Molecular mechanisms of neonatal brain injury. Neurol Res Int 506320:1–16. doi:10.1155/2012/506320
2. Zhang DW, Shao J, Lin J, Zhang N, Lu BJ, Lin SC, Dong MQ, Han J (2009) RIP3, an energy metabolism regulator that switches TNF-induced cell death from apoptosis to necrosis. Science 325:332–336. doi:10.1126/science.1172308
3. He S, Wang L, Miao L, Wang T, Du F, Zhao L, Wang X (2009) Receptor interacting protein kinase-3 determines cellular necrotic response to TNF-alpha. Cell 137:1100–1111. doi:10.1016/j.cell.2009.05.021
4. Fayaz SM, Suvanish Kumar V, Rajanikant GK (2014) Necroptosis: who knew there were so many interesting ways to die? CNS Neurol Disord Drug Targets 13:42–51. doi:10.2174/18715273113126660189
5. Linkermann A, Hackl MJ, Kunzendorf U, Walczak H, Krautwald S, Jevnikar AM (2013) Necroptosis in immunity and ischemia reperfusion injury. Am J Transplant 13:2797–2804. doi:10.1111/ajt.12448
6. Mehta SL, Manhas N, Raghubir R (2007) Molecular targets in cerebral ischemia for developing novel therapeutics. Brain Res Rev 54:34–66. doi:10.1016/j.brainresrev.2006.11.003
7. Meylan E, Burns K, Hofmann K, Blancheteau V, Martinon F, Kelliher M, Tschopp J (2004) RIP1 is an essential mediator of Toll-like receptor3-induced NF-kB activation. Nat Immunol 5:503–507. doi:10.1038/ni1061
8. Linkermann A, Green DR (2014) Necroptosis. N Engl J Med 370:455–465. doi:10.1056/NEJMra1310050
9. Vandenabeele P, Galluzzi L, Vanden Berghe T, Kroemer G (2010) Molecular mechanisms of necroptosis: an ordered cellular explosion. Nat Rev Mol Cell Biol 11:700–714. doi:10.1038/nrm2970
10. Chan FK, Shisler J, Bixby JG, Felices M, Zheng L, Appel M, Orenstein J, Moss B, Lenardo MJ (2003) A role for tumor necrosis factor receptor-2 and receptor-interacting protein in programmed necrosis and antiviral responses. J Biol Chem 278:51613–51621. doi:10.1074/jbc.M305633200
11. Holler N, Zaru R, Micheau O, Thome M, Attinger A, Valitutti S, Bodmer JL, Schneider P, Seed B, Tschopp J (2000) Fas triggers an alternative, caspase-8-independent cell death pathway using the kinase RIP as effector molecule. Nat Immunol 1:489–495. doi:10.1038/82732
12. Lin Y, Choksi S, Shen HM, Yang QF, Hur GM, Kim YS, Tran JH, Nedospasov SA, Liu ZG (2004) Tumor necrosis factor induced non-apoptotic cell death requires receptor-interacting protein-mediated cellular reactive oxygen species accumulation. J Biol Chem 279:10822–10828. doi:10.1074/jbc.M313141200
13. Ch'en IL, Tsau JS, Molkentin JD, Komatsu M, Hedrick SM (2011) Mechanisms of necroptosis in T cells. J Exp Med 208:633–641. doi:10.1084/jem.20110251
14. Degterev A, Huang Z, Boyce M, Li Y, Jagtap P, Mizushima N, Cuny GD, Mitchison TJ, Moskowitz MA, Yuan J (2005) Chemical inhibitor of nonapoptotic cell death with therapeutic potential for ischemic brain injury. Nat Chem Biol 1:112–119. doi:10.1038/nchembio711
15. Smith CC, Davidson SM, Lim SY, Simpkin JC, Hothersall JS, Yellon DM (2007) Necrostatin: a potentially novel cardioprotective agent? Cardiovasc Drugs Ther 21:227–233. doi:10.1007/s10557-007-6035-1
16. Xu X, Chua CC, Kong J, Kostrzewa RM, Kumaraguru U, Hamdy RC, Chua BH (2007) Necrostatin-1 protects against glutamate induced glutathione depletion and caspase-independent cell death in HT-22 cells. J Neurochem 103:2004–2014. doi:10.1111/j.1471-4159.2007.04884.x
17. Bao L, Li Y, Deng SX, Landry D, Tabas I (2006) Sitosterol containing lipoproteins trigger free sterol-induced caspase-independent death in ACAT-competent macrophages. J Biol Chem 281:33635–33649. doi:10.1074/jbc.M606339200
18. Hong Q, Hsu LJ, Schultz L, Pratt N, Mattison J, Chang NS (2007) Zfra affects TNF-mediated cell death by interacting with death domain protein TRADD and negatively regulates the activation of NF-kappaB, JNK1, p53 and WOX1 during stress response. BMC Mol Biol 8:50. doi:10.1186/1471-2199-8-50
19. Degterev A, Hitomi J, Germscheid M, Ch'en IL, Korkina O, Teng X, Abbott D, Cuny GD, Yuan C, Wagner G, Hedrick SM, Gerber SA, Lugovskoy A, Yuan J (2008) Identification of RIP1 kinase as a specific cellular target of necrostatins. Nat Chem Biol 5:313–321. doi:10.1038/nchembio.83
20. Ch'en IL, Beisner DR, Degterev A, Lynch C, Yuan J, Hoffmann A, Hedrick SM (2008) Antigen-mediated T cell expansion regulated by parallel pathways of death. Proc Natl Acad Sci USA 105:17463–17468. doi:10.1073/pnas.0808043105
21. Ting AT, Pimentel-Muinos FX, Seed B (1996) RIP mediates tumor necrosis factor receptor 1 activation of NF-kappaB but not Fas/APO-1-initiated apoptosis. EMBO J 15:6189–6196
22. Kaiser WJ, Upton JW, Long AB, Livingston-Rosanoff D, Daley-Bauer LP, Hakem R, Caspary T, Mocarski ES (2011) RIP3 mediates the embryonic lethality of caspase-8-deficient mice. Nature 471:368–372. doi:10.1038/nature09857
23. Oberst A, Dillon CP, Weinlich R, McCormick LL, Fitzgerald P, Pop C, Hakem R, Salvesen GS, Green DR (2011) Catalytic activity of the caspase-8-FLIP(L) complex inhibits RIPK3-dependent necrosis. Nature 471:363–367. doi:10.1038/nature09852
24. Vanlangenakker N, Bertrand MJ, Bogaert P, Vandenabeele P, VandenBerghe T (2011) TNF induced necroptosis in L929 cells is tightly regulated by multiple TNFR1 complex I and II members. Cell Death Dis 2:e230. doi:10.1038/cddis.2011.111

25. Zou J, Xie HZ, Yang SY, Chen JJ, Ren JX, Wei YQ (2008) Towards more accurate pharmacophore modeling: multicomplex based comprehensive pharmacophore map and most-frequent feature pharmacophore model of CDK2. J Mol Graph Model 27:430–438. doi:10.1016/j.jmgm.2008.07.004
26. Fayaz SM, Rajanikant GK (2014) Ensemble pharmacophore meets ensemble docking: a novel screening strategy for the identification of RIPK1 inhibitors. J Comput Aided Mol Des 28:779–794. doi:10.1007/s10822-014-9771-x
27. Nair SB, Fayaz SM, Rajanikant GK (2013) A novel multi-target drug screening strategy directed against key proteins of DAPk family. Comb Chem High Throughput Screen 16:449–457. doi:10.2174/1386207311316060005
28. Darden T, York D, Pedersen L (1993) Particle mesh Ewald—an N.log(N) method for Ewald sums in large systems. J Chem Phys 98:10089–10093. doi:10.1063/1.464397
29. Friesner RA, Banks JL, Murphy RB, Halgren TA, Klicic JJ, Mainz DT, Repasky MP, Knoll EH, Shelley M, Perry JK, Shaw DE, Francis P, Shenkin PS (2004) Glide: a new approach for rapid, accurate docking and scoring. 1. Method and assessment of docking accuracy. J Med Chem 47:1739–1749. doi:10.1021/jm0306430
30. Salam NK, Nuti R, Sherman W (2009) Novel method for generating structure-based pharmacophores using energetic analysis. J Chem Inf Model 49:2356–2368. doi:10.1021/ci900212v
31. Irwin JJ, Shoichet BK (2005) ZINC—a free database of commercially available compounds for virtual screening. J Chem Inf Model 45:177–182. doi:10.1021/ci049714+
32. Bender A, Glen RC (2005) A discussion of measures of enrichment in virtual screening: comparing the information content of descriptors with increasing levels of sophistication. J Chem Inf Model 45:1369–1375. doi:10.1021/ci0500177
33. Jain AN, Nicholls A (2008) Recommendations for evaluation of computational methods. J Comput Aided Mol Des 22:133–139. doi:10.1007/s10822-008-9196-5
34. Hamza A, Wei NN, Zhan CG (2012) Ligand-based virtual screening approach using a new scoring function. J Chem Inf Model 52:963–974. doi:10.1021/ci200617d
35. van Aalten DM, Bywater R, Findlay JB, Hendlich M, Hooft RW, Vriend G (1996) PRODRG, a program for generating molecular topologies and unique molecular descriptors from coordinates of small molecules. J Comput Aided Mol Des 10:255–262. doi:10.1007/BF00355047
36. Humphrey W, Dalke A, Schulten K (1996) VMD: visual molecular dynamics. J Mol Graph 14:33–38. doi:10.1016/0263-7855(96)00018-5